JOURNAL OF SOLID STATE CHEMISTRY 108, 219–229 (1994)

The Substitution of CO_3 Groups for Copper in $Y_{1-x}Ca_xBa_2Cu_3O_7$: HREM Study

B. Domengès, Ph. Boullay, M. Hervieu, and B. Raveau

Laboratoire CRISMAT ISMRA/Université de Caen, Bd. du Maréchal Juin, 14050 Caen Cedex, France

Received March 22, 1993; accepted May 17, 1993

The carbonation of the 123-type cuprates $(Y_{1-x}Ca_x)_nBa_{2n}Cu_{3n-1}CO_3O_{7n-3}$ has been studied by high-resolution electron microscopy. The investigation of the system, varying x and n, shows that the most stable phase is the $n = 2$ member. A structural model is proposed from XRD profile analysis for $Y_{1.3}Ca_{0.7}Ba_4Cu_5CO_3O_{11}$. The contrast of the HREM images was calculated on the basis of the XRD data and is discussed depending on focus values, carbon substitution, and crystal thickness. The study of the distribution of the CO_3 groups versus composition shows that different n members are locally stabilized, from $n = 1$ to $n = \infty$. Short thermal treatments involve the formation of local ordering, in domains of some tens of angströms width, which correspond to local superstructures along [110] and [031]; 90° oriented domains are frequent phenomena in these materials, and the boundaries are generally parallel to (001). Some intergrowth defects, in the form of "124" members, are observed.

INTRODUCTION

The understanding of the **123** cuprates is a very important issue owing to the potential applications of the 92-K superconductor $YBa_2Cu_3O_7$. The partial replacement of copper by carbonate groups in the **123** structure was first evidenced in the strontium-based cuprates $YSr_2Cu_3O_7$ (1) and $Y_{1-x}Ca_xSr_2Cu_3O_7$ (2). The recent synthesis and HREM study of the oxycarbonate $Y_4Sr_8Cu_{11}CO_3O_{25}$ (3) have shown that this **123** derivative results from an ordered substitution of one row of $Cu(1)O_4$ groups out of four, leading to a "$4a_{123} \times b \times 2c_{123}$" superstructure. In such a substitution, the triangular CO_3 groups then share two apical oxygens with the $Cu(2)O_5$ pyramids, whereas the third corner is directed toward the adjacent CuO_4 groups, so that rows of CuO_4 groups are replaced by rows of CuO_5 pyramids at the level of Cu(1). This substitution may take place without any variation of the total oxygen content, so that a series of new phases, with the generic formula $(Y_{1-x}Ca_x)_n(Ba,Sr)_{2n}Cu_{3n-1}CO_3O_{7n-3}$ has been predicted (4), characterized by different superstructures according to the n value. This ordering model allows the "$4a_{123} \times b_{123} \times 2c_{123}$," "$3a_{123} \times b_{123} \times 2c_{123}$," and "$2a_{123} \times b_{123} \times 2c_{123}$" supercells observed in the Sr-based systems (1–3) to be explained.

The introduction of CO_3 groups in the pure barium **123** cuprates has only been shown recently with the synthesis of the oxycarbonate $(Y_{1-x}Ca_x)_2Ba_4Cu_5CO_3O_{11}$ (5), characterized by the supercell "$2a_{123} \times b_{123} \times 2c_{123}$," corresponding to the second member of the series. In order to understand the eventual formation of other members of this series and the distribution of CO_3 groups in the matrix in connection with order–disorder phenomena, the systematic exploration of this system corresponding to the compositions $(Y_{1-x}Ca_x)_nBa_{2n}Cu_{3n-1}CO_3O_{7n-3}$ is necessary. We report here on the high-resolution electron microscopy study of different samples with $0.1 \leq x \leq 0.6$ and $2 \leq n \leq 6$.

EXPERIMENTAL

Several samples were prepared varying the Y/Ca ratio with $0.1 < x \leq 0.6$ and the n value from $n = 2$ to $n = 6$.

The starting products were Y_2O_3, CaO, $BaCO_3$, BaO_2, CuO, and $BaCuO_2$; the mixtures were intimately ground in an agate mortar and sealed in an evacuated silica tube. The O_2 and CO_2 partial pressures were varied by changing the $BaCO_3/BaO_2/BaCuO_2$ ratios. Samples were heated at 900°C for 24 h to 15 days, and the temperature was slowly decreased down to ambiant.

The powder X-ray diffraction patterns were registered on a Seifert diffractometer with CuK_α radiation. The samples for electron microscopy were prepared by soft grinding in n-butanol and the grains were deposited on holey carbon coated grids. The electron diffraction study was performed with a Jeol 200 CX electron microscope fitted with a eucentric goniometer (±60°) and the high-resolution work with a Topcon 002 B microscope equipped with a double-tilt sample holder (±10°) and an objective lens with spherical aberration constant $C_s = 0.4$ mm. The HREM images were calculated using the multislice method of the EMS program (6).

0022-4596/94 $6.00

The EDS analyses were performed with Kevex analyzers mounted on both microscopes.

RESULTS AND DISCUSSION

Whatever the nominal composition (x, n) may be, the powder X-ray diffraction patterns evidence the **123**-type phase but with weak extra reflections. The electron diffraction analysis confirms this observation and shows that in any sample only one type of superstructure is observed characterized by the orthorhombic supercell "$2a_{123} \times a_{123} \times {}^2c_{123}$," as shown from the [010], [100], and [001] ED patterns (Fig. 1). However, the intensity of the extra reflections decreases when n increases. Moreover, it must be pointed out that no other phase was detected for the various samples, except for very small amounts of $BaCO_3$ which could never be eliminated. This preliminary study suggests that the most stable phase of this system is the $n = 2$ member $(Y_{1-x}Ca_x)_2Ba_4Cu_5CO_3O_{11}$. However, it raises the issue of the distribution of the carbonate groups for other n values, since we did not observe any mixture of the pure **123** phase $YBa_2Cu_3O_7$ with this $n = 2$ member. The systematic HREM investigation of various samples solves this problem.

EDS analyses of tens of microcrystals in several samples show that Y–Ca–Ba composition follows a distribution centered on a mean composition close to the synthesis composition when $x \leq 0.4$. For instance, in $x = 0.4$–$n = 2$ samples, the analyzed cation ratios of 24 microcrystals lead to the mean formulation $Y_{0.71(0.12)}Ca_{0.35(0.11)}Ba_{1.94(0.07)}$ (standard deviations are given) which suggests that part of the substituted Ca atoms occupies Ba sites. In $x = 0.6$–$n = 2$ samples, the analyzed mean composition is $Y_{0.66(0.16)}Ca_{0.40(0.14)}Ba_{1.94(0.09)}$, leading to the same remark concerning the substitution of Ca atoms on Ba sites. Also, though the mean composition on Y site is given by a Y/Ca ratio equal to 2, some crystals were analyzed to $Y_{0.5}Ca_{0.5}Ba_{2.0}$, showing that it is possible to substitute up to half of the Ca for Y.

The $n = 2$ Member $Y_{1.3}Ca_{0.7}Ba_4Cu_5CO_3O_{11}$: Structural Model

The interpretation of the HREM experimental contrast of the images of the various samples requires a comparison with simulated images based on a structural model. For this reason we have first established a structural model from XRD profile analysis for the $n = 2$ member $Y_{1.3}Ca_{0.7}Ba_4Cu_5CO_3O_{11}$, which is used as a reference.

As for all other samples, the reconstruction of the reciprocal space of this phase from ED patterns leads to an orthorhombic supercell, with the reflection conditions $h\ k\ l$, $h + l = 2n$, corresponding to the possible space groups $B222$, $Bm2m$, and $Bmmm$. The powder XRD patterns, which show clearly weak superstructure lines, were then indexed in the orthorhombic cell with the following parameters:

$$a = 7.770(1)\ \text{Å}, \quad b = 3.888(1)\ \text{Å}, \quad \text{and } c = 22.981(1)\ \text{Å}.$$

Note the pseudotetragonal character of the subcell, shown by the $(a/2)/b$ ratio close to 1. We also observe that the c/a ratio is significantly smaller than 3, contrary to $YBa_2Cu_3O_7$ and $Y_{1-x}Ca_xBa_2Cu_3O_{7-\delta}$. This feature is easily explained by the substitution of CO_3 groups for Cu(1), which brings the Cu(2) layers closer together.

The mean structure was first studied in the **123** subcell and then the structure calculations were performed in the $Bm2m$ space group of the supercell, introducing $BaCO_3$ as an impurity. The starting atomic positions are deduced from the $YBa_2Cu_3O_7$ structure (Fig. 2a) by replacing one row of CuO_4 groups (Cu(1)) out of two by one row of CO_3 groups in an ordered way. The CO_3 groups were supposed to be statistically oriented toward the adjacent CuO_4 groups. Consequently, the occupancy factor of the O(7) site, shared between one CO_3 group and one Cu(1) polyhedron was arbitrary fixed to 0.50 (Fig. 2b). All the isotropic parameters of oxygen atoms and carbon were fixed to 1 Å^2. Only the positional parameters of the metallic atoms and oxygen atoms were refined. The profile agreement

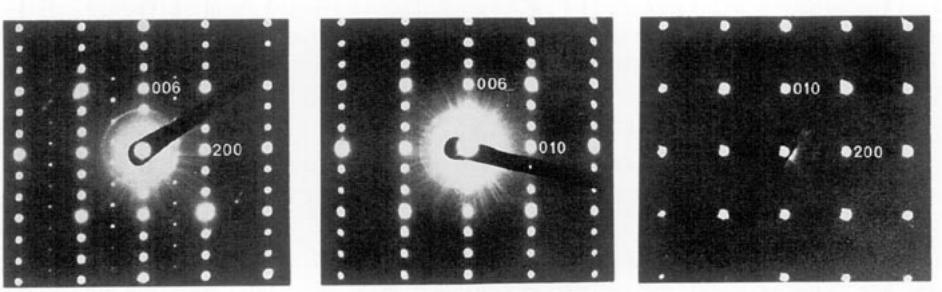

FIG. 1. [010], [100], and [001] ED patterns showing reflection conditions $h\ k\ l$, $h + l = 2n$, characteristic of the B lattice.

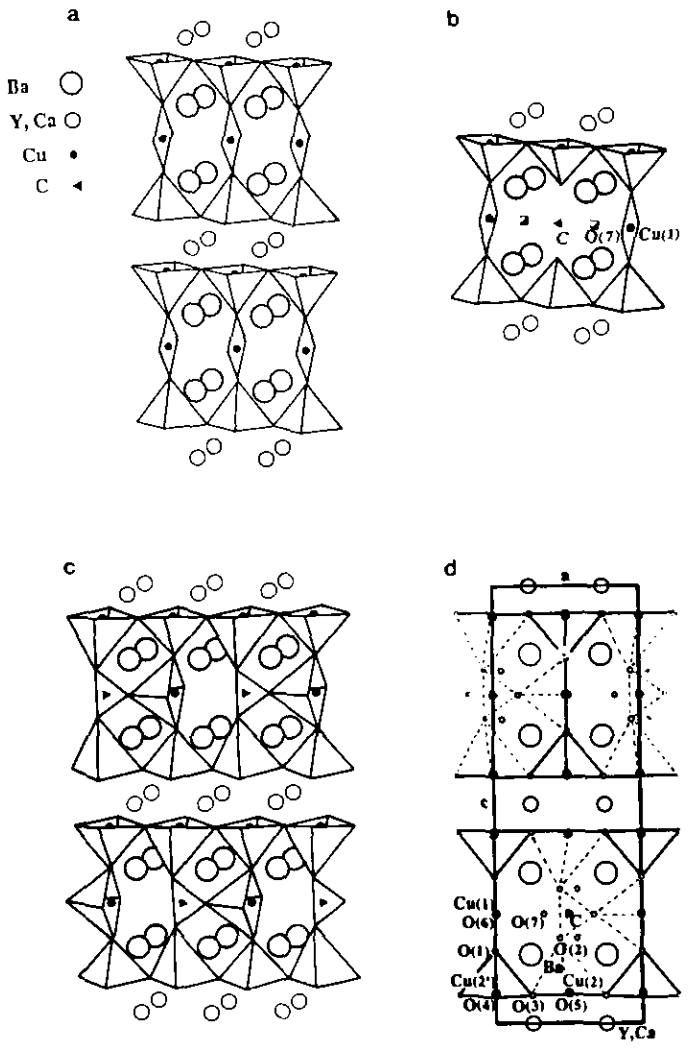

FIG. 2. Perspective views of **123** related structures: (a) $YBa_2Cu_3O_7$; (b) carbonated **123**, O(7) site is half occupied; (c) perfectly ordered **123** *oxycarbonate*; and (d) [010] *projection* of $Y_{1.3}Ca_{0.7}Ba_4Cu_5CO_3O_{11}$.

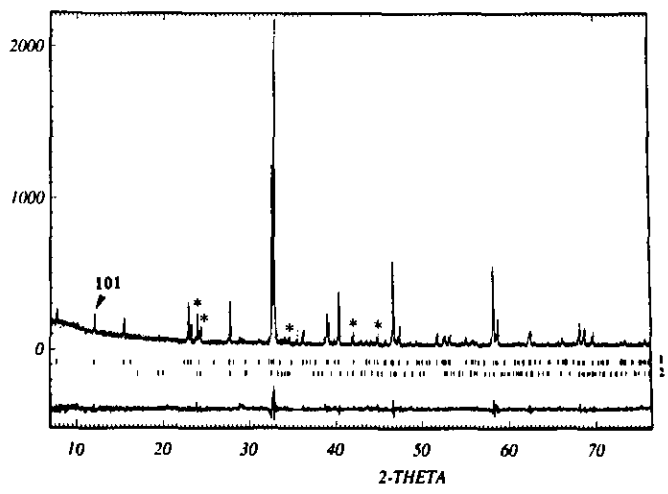

FIG. 3. Observed, calculated, and difference XRD powder patterns. Reflections are located in (1) for the $Y_{1.3}Ca_{0.7}Ba_4Cu_5CO_3O_{11}$ compound and in (2) for the $BaCO_3$ secondary phase. The strongest reflection characteristic of the superstructure is 101. The five strongest reflections of the $BaCO_3$ secondary phase are indicated by an asterisk.

factors were stabilized to $R_p = 10.6\%$, $R_{wp} = 14.6\%$, and $R_i = 6.6\%$ (XRD powder pattern is given in Fig. 3) for the data of Table 1.

Though the positions of the oxygen and carbon atoms cannot be considered as accurate, these results show the validity of our structural model. For a perfectly ordered structure, all the CO_3 groups would be oriented in the same direction so that at the level of Cu(1), the structure would be described as a regular stacking of rows of CuO_5 pyramids and of CO_3 groups alternately along $\vec{a}$ (Fig. 2c). A random distribution of oxygen on the O(7) sites (and thus O(2)) can be explained by a change of the orientation of the different rows of CO_3 groups, leading to the coexistence of rows of CuO_4 square groups, CuO_5 pyramids, and CuO_6 octahedra in the same crystal. XRD data, as well as HREM simulation, do not allow these two extreme models to be differenciated. In any case, these rows of CO_3 and CuO_4 groups form mixed layers which are stacked along $\vec{c}$ in such a way that two successive layers are shifted with respect to each other of $a/2$.

TABLE 1

$Y_{1.3}Ca_{0.7}Ba_4Cu_5CO_3O_{11}$: Structural Parameters $a = 7.7704(6)$ Å, $b = 3.8876(3)$ Å, $c = 22.9812(8)$ Å; Space Group $Bm2m$[a]

Atom	Site	x	y	z	B (Å^2)
$Y_{0.65}Ca_{0.35}$	4c	0.25	0.5	0.0	0.3(2)
Ba	8*f*	0.2414(8)	0.5	0.1566(1)	1.0(1)
C	2*b*	0.5	0.0	0.25	1
Cu(1)	2*a*	0.0	0.0	0.25	0.7(5)
Cu(2)[b]	4*c*	0.5	0.0	0.0690(2)	0.4(2)
Cu(2')[b]	4*e*	0.0	0.0	0.0690(2)	0.4(2)
O(1)	4*e*	0.0	0.0	0.165(2)	1
O(2)[c]	8*f*	0.44	0.0	0.194	1
O(3)	8*f*	0.25	0.0	0.065(8)	1
O(4)[b]	4*c*	0.0	0.5	0.061(8)	1
O(5)[b]	4*e*	0.5	0.5	0.061(8)	1
O(6)	2*a*	0.0	0.5	0.25	1
O(7)[c]	4*d*	0.67	0.0	0.25	1

Note. $R_p = 10.6\%$, $R_{wp} = 14.6\%$, $R_{exp} = 12.1\%$, $R_i = 6.6\%$, and $\chi^2 = 1.47$.

[a] In order to keep the same origin as the **123** structure, a translation of 0 0 ¼ has been performed, i.e., a mirror plane perpendicular to *c* sits at $z = \frac{1}{4}$ and $\frac{3}{4}$ (instead of 0 and $\frac{1}{2}$).

[b] *z* parameters of Cu(2) and Cu(2') are strongly correlated; they were constrained to the same variation and *B* parameter. The same remark applies to z(O(4)) and z(O(5)).

[c] Nonrefined parameters; $\sigma = 0.5$ to allow both possible orientations of CO_3 groups.

However, the powder XRD study allows some important points to be emphasized:

(i) the ordered substitution of carbon for Cu(1) is significant. Indeed, the introduction of copper on the carbon sites leads to an increase of R_i up to 14.5%;

(ii) the z positions of the two different sites Cu(2) and Cu(2′) which correspond to the pyramidal layers (Fig. 2d) are identical contrary to what is observed by Myazaki *et al.* (1) in the strontium-based **123** oxycarbonate, which is characterized by a puckering of the $[CuO_2]_\infty$ layers;

(iii) barium atoms are displaced from their ideal positions, moving away from the O(7) site shared by the CO_3 group and one Cu(1) polyhedron;

(iv) the interatomic distances calculated for this model (Table 2) are close to these usually observed, particularly for the apical Cu(1)–O distances of the CuO_6 or CuO_5 pyramids and the Cu(2)–O apical distances of the CuO_5 pyramids.

Calculated images. This structural model allows calculations to be performed for the simulation of HREM images. As previously mentioned (3) the best orientation to image these oxycarbonates is that of [010]. An example of [010] image recorded for different focus values is given in Fig. 4. Two important features must be pointed out:

(i) the contrast is closely related to that of the **123** structure, but the rows of carbonate groups can be clearly identified;

(ii) the undulations of the $[CuO_2]_\infty$ layers which were observed for $Y_4Sr_8Cu_{11}CO_3O_{25}$ (3) are not visible here. This supports strongly the XRD results which show flat $[CuO_2]_\infty$ layers.

TABLE 2

$Y_{1.3}Ca_{0.7}Ba_4Cu_5CO_3O_{11}$: Interatomic Distances (Å)

Y,Ca–O(3)	4 × 2.45		
O(4)	2 × 2.40		
O(5)	2 × 2.40		
Ba–O(1)	2.71		
O(2)	2 × 2.63		
O(3)	2 × 2.86		
O(4)	2.88		
O(5)	2.97		
O(6)	2.85		
O(7)	2.98		
C–O(2)	1.36	O(2)–C–O(2)	140.3°
O(7)	1.32	O(2)–C–O(7)	109.9°
Cu(1)–O(1)	2 × 1.94		
O(6)	2 × 1.94		
O(7)	2.56		
Cu(2)–O(2)	2.91		
O(3)	2 × 1.95		
O(5)	2 × 1.95		
Cu(2′)–O(2)	2.22		
O(3)	2 × 1.95		
O(5)	2 × 1.95		

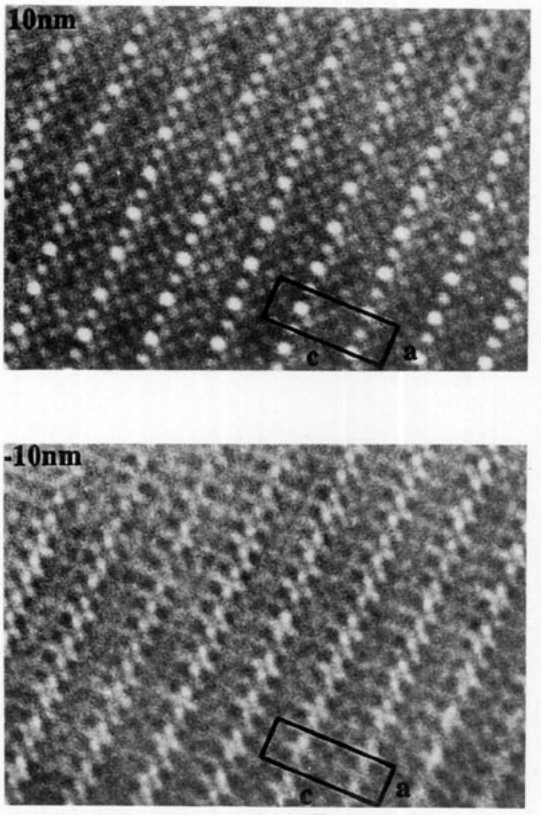

FIG. 4. [010] HREM images observed for two focus values characteristic of carbon substitution of Cu(1).

The calculated through-focus series for thin crystals (Fig. 5A) show that several focus values allow us to distinguish carbon-substituted rows from noncarbonated ones. However, a careful examination of the contrast, and especially its evolution with crystal thickness, shows that few images will be indicative of carbon substitution. This effect is probably due to the absence of strong displacement of cations surrounding carbon atoms, contrary to **123**-Sr-based carbonates where a waving of atom rows was observed related to carbon substitution and which led to a stronger dependence of contrast. One of the most sensitive images to carbon substitution is obtained for a slight overfocus. At a 10-nm focus, cation rows appear as bright spots: three rows of brighter spots, corresponding to barium and mixed copper–carbon rows, alternate with three rows of grayer ones, corresponding to yttrium–calcium and pyramidal copper rows. Along the mixed copper–carbon rows, carbons appear as brighter dots, so that one of every two dots is highlighted, leading to centered $2a \times 2c$ array. A second characteristic image is observed for a −10-nm focus value. There, low-electron-density zones are highlighted and in the carbon rows oxygen atoms surrounding carbon appear in the form of four bright dots in a 0.27×0.27 nm^2 square. This contrast, which was also characteristic of carbon substitution in

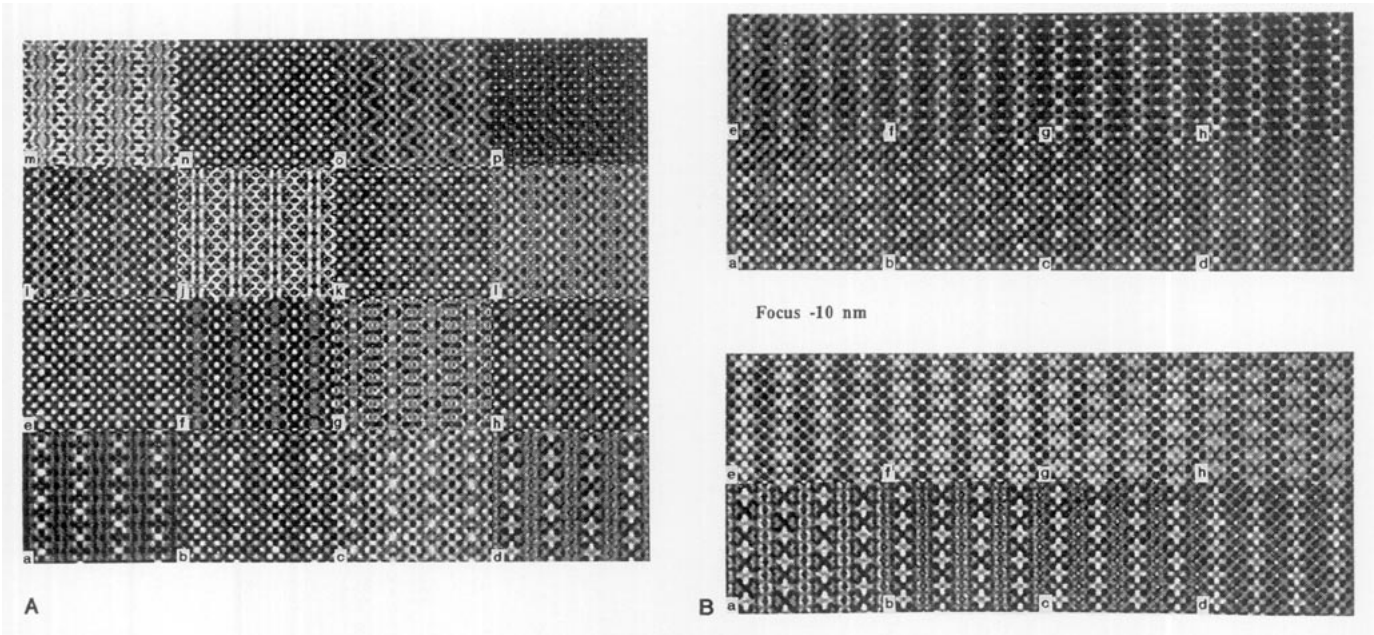

FIG. 5. [010] HREM calculated images for $Y_{0.65}Ca_{0.35}Ba_2Cu_{2.5}C_{0.5}O_7$. Calculation parameters are high voltage $V = 200$ kV, spherical aberration constant $C_s = 0.4$ mm, half angle convergence $\alpha/2 = 0.85$ mrad, spread of focus $\Delta = 10$ nm. In (A) the crystal thickness is fixed to 3.1 nm and focus varies from (a) 20 nm to (o) − 120 nm (by 10-nm steps); (p) is the [010] projected potential of the structure. In (B) the crystal thickness varies from (a) 2.3 nm to (h) 7.8 nm (by 0.78-nm steps) for two focus values.

123-Sr-based carbonates, is not any greater when crystal thickness increases ($T > 4$ nm) (Fig. 5B). Experimental image observation led to the same remarks on contrast dependence on carbon substitution, and crystal thickness appeared to be an important factor to consider. Slight overfocus corresponds thus to the optimum observation conditions for carbon substitution enhancement.

The Distribution of CO_3 Groups versus Composition: Intergrowth of Different n Members of the Family $(Y_{1-x}Ca_x)_nBa_{2n}Cu_{3n-1}CO_3O_{7n-3}$

For the ideal composition, $n = 2$, the "$2a_{123} \times 2c_{123}$" superstructure is established on large domains, as shown in Fig. 6a; besides these large domains, one observes a contrast characteristic of the **123** structure, which can be explained by the fact that part of the oxycarbonate is decomposed during the synthesis leading to (Y,Ca)$Ba_2Cu_3O_{7-\delta}$ ($n = \infty$).

For $n > 2$, we observe that the "$2a_{123} \times 2c_{123}$" superstructure is only established as more less extended domains in a classical **123**-type matrix. An example is shown in Fig. 6b for a nominal composition $n = 6$ and $x = 0.2$. The typical contrast of the ordered white dots, correlated to the existence of CO_3 groups, is only observed in the bottom right part of the image, in a domain labeled ①; in the domain labeled ②, the contrast which is observed is that of the **123** structure. Thus in the majority of the crystals, the compositions corresponding to $n > 5$ consist mainly of domains of the oxycarbonate $(Y_{1-x}Ca_x)_2Ba_4Cu_5CO_3O_{11}$ intergrown in **123** matrix $Y_{1-x}Ca_xBa_2Cu_3O_{7-\delta}$.

In domains where the $2a_{123} \times 2c_{123}$ superstructure is established we sometimes observe breaking in the regularity of the carbon–copper atom arrangement (Fig. 7).

In Fig. 7a, we observe a zone (arrowed) where a "$3a_{123}$" periodicity is established along $\vec{a}$: for each row at the level of the mixed layer, one white dot alternates with two gray dots along $\vec{a}$. Such an order is correlated to the sequence of one carbonate group and two copper polyhedra along the $\vec{a}$ axis, as shown in the idealized model; such an ordering corresponds to the member $n = 3$ of the family which can be formulated $(YCa)_3Ba_6Cu_8CO_3O_{19}$.

In Fig. 7b, complete rows of white dots are running along $\vec{a}$ (double arrowed); such a contrast could be correlated to the formation of local zones where all the Cu(1) atoms are substituted by carbon. Such a member would correspond to $(Y_{1-x}Ca_x)Ba_2Cu_2CO_3O_4$, i.e., to the $n = 1$ member (see idealized model). In the same image, another interesting feature must be emphasized: at the level of the single arrow, we observe a new periodicity which corresponds to a "$2a_{123} \times 1c_{123}$" superstructure. This means that the rows of groups CO_3 and CuO_5 pyramids alternate along $\vec{a}$ exactly as described above for $n = 2$, but that two successive (001) mixed layers of CO_3 and CuO_4 groups are not shifted with respect to each other along $\vec{a}$. Thus this ordering appears as a second form of

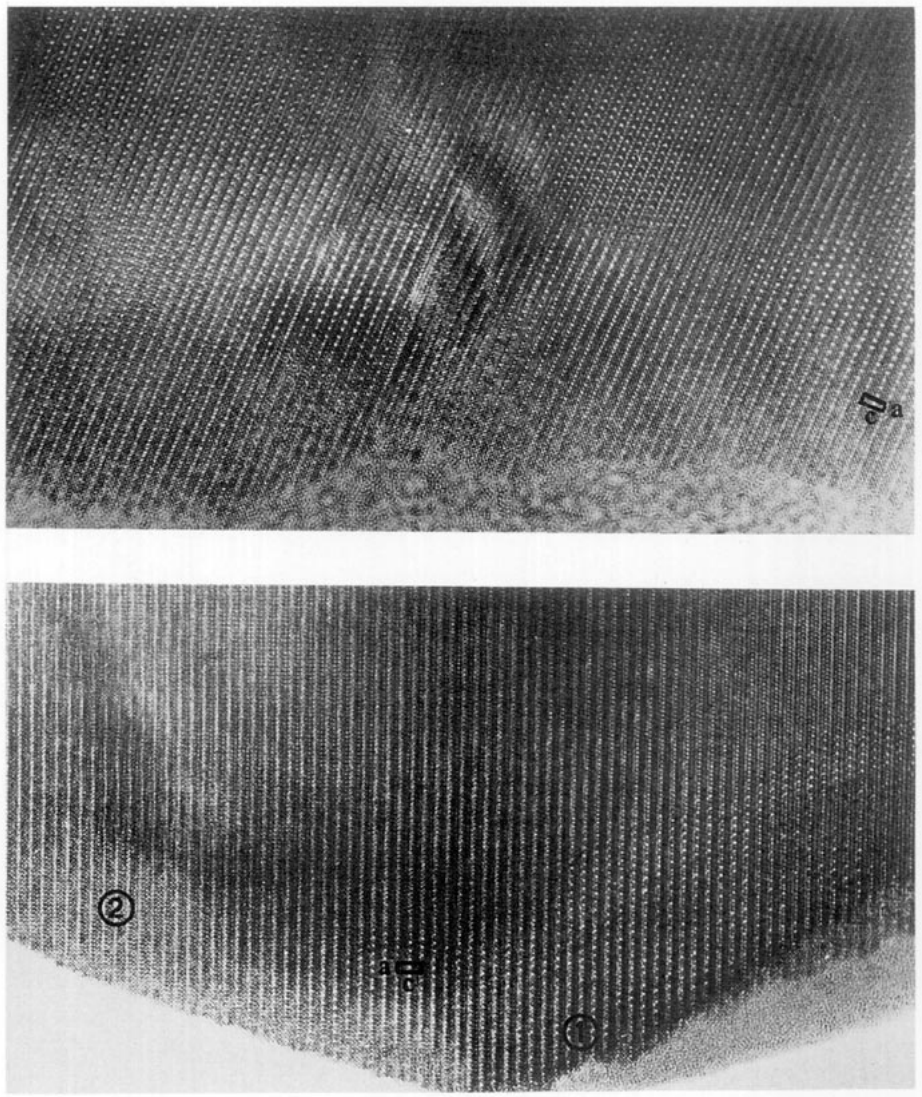

FIG. 6. (a) [010] HREM image of a microcrystal ($Y_{1.6}Ca_{0.4}Ba_2Cu_5CO_3O_{11}$ batch) showing a well established "$2a_{123} \times 2c_{123}$" superstructure (focus close to 10 nm). (b) [010] HREM image of a microcrystal ($Y_{4.8}Ca_{1.2}Ba_{12}Cu_{17}CO_3O_{39}$ batch) showing two domains (focus close to 10 nm): in ① the "$2a \times 2c$" superstructure is well established, which corresponds to the formulation $Y_{1.6}Ca_{0.4}Ba_4Cu_5CO_3O_{11}$, whereas domain ② does not exhibit any superstructure, that is, does not contain any carbon and is $(Y,Ca)Ba_2Cu_3O_7$ type.

the $n = 2$ member characterized by a similar composition $(Y,Ca)_2Ba_4Cu_5CO_3O_{11}$.

Other Local Ordering

For short thermal treatments (1 or 2 days), the samples often exhibit local ordering, in domains of some tens of Angströms width. They are especially visible when the crystals are viewed along [001]. One example is shown in Fig. 8a, where the local superstructure is $a' = 3a_{123}\sqrt{2}$ and $b' = a_{123}\sqrt{2}$. Such a supercell cannot be explained by any model based on carbon–copper ordering phenomenon. Local ordering are also observed along [100] as in Fig. 8b, where modulation of the contrast appears parallel to $(013)_{123}$ with two- and threefold periodicities. In this image, the contrast consists of one row of white dots separated by three alternating rows of small dots which are correlated to the Cu–Y–Cu layers of the structure; it appears that this modulation especially affects these three rows where the atoms are displaced.

When the samples were heated for a long time the [001] images did not exhibit such modulations or Moiré patterns.

Such phenomena could be correlated to order–disorder phenomena at the level of the Y–Ca layer which are favored by short heating times.

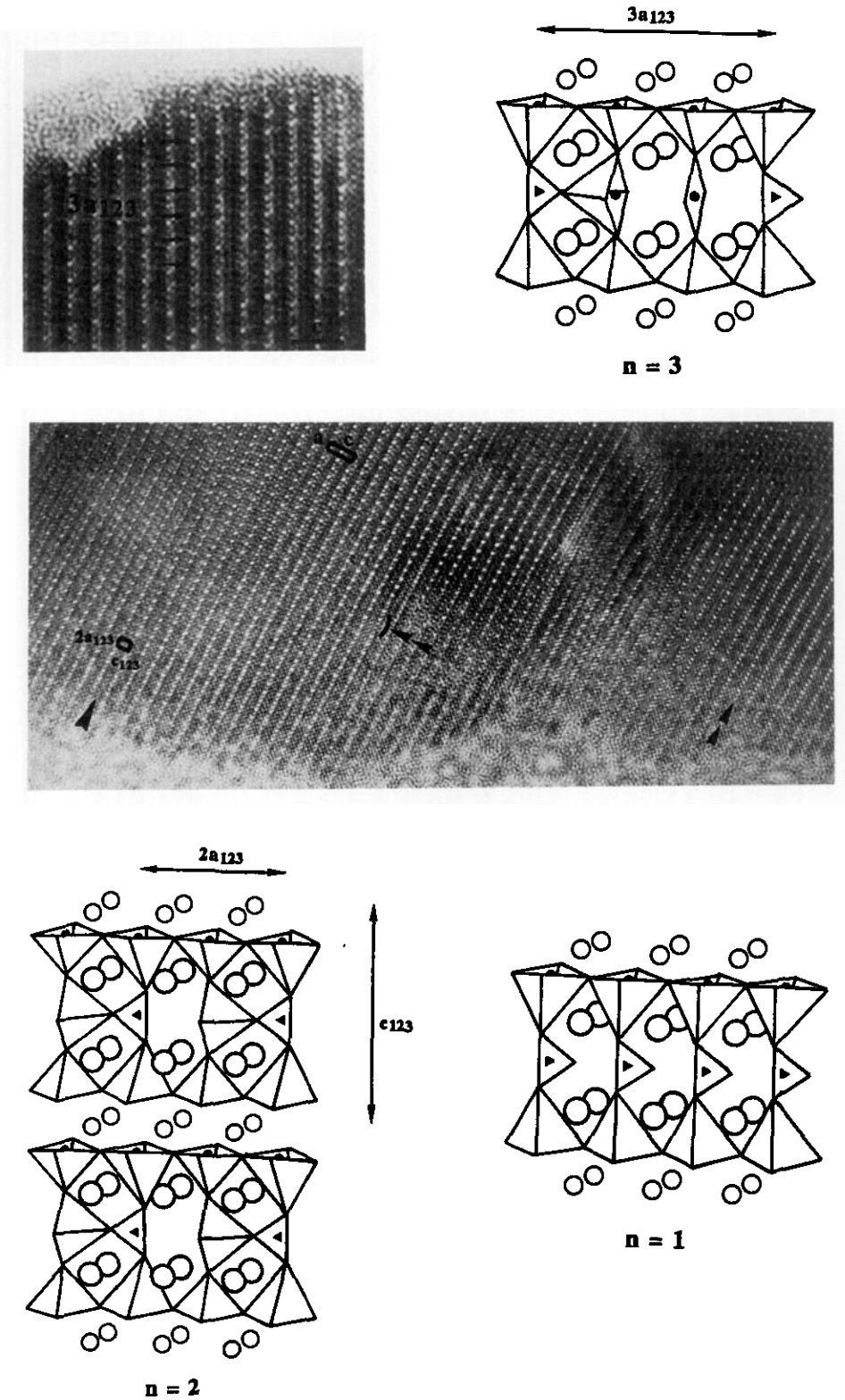

FIG. 7. (a) Detail of [010] HREM image of a microcrystal ($x = 0.2$, $n = 6$ batch) taken at focus close to 10 nm. Bright dots corresponding to carbon atoms follow a $3a_{123}$ periodicity. Perspective view of corresponding structural model $n = 3$ member. (b) [010] HREM image of a microcrystal ($x = 0.2$, $n = 2$ batch), taken at focus close to 10 nm, showing in a regular $2a_{123} \times 2c_{123}$ matrix two types of defective slabs. In the first one (double arrowed) bright dots related to substituted carbon atoms follow the periodicity a_{123}. In the second one (big arrow) bright dots form a $2a_{123} \times c_{123}$ array; perspective view of corresponding structural model $n = 1$ member and second form of $n = 2$ member.

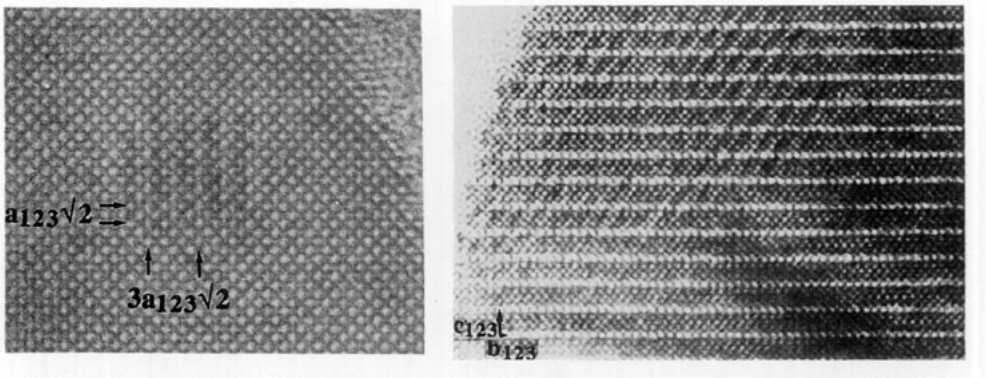

FIG. 8. Detail of [001] HREM image of a microcrystal ($x = 0.2$, $n = 2$ batch) showing a 3.9 × 3.9 Å^2 square array of bright dots. On a small domain (30 × 30 Å^2) brighter dots form a centered $a_{123}\sqrt{2} \times 3a_{123}\sqrt{2}$ array. (b) [100] HREM image of a microcrystal ($x = 0.2$, $n = 6$ batch) showing a modulation of contrast parallel to $(013)_{123}$.

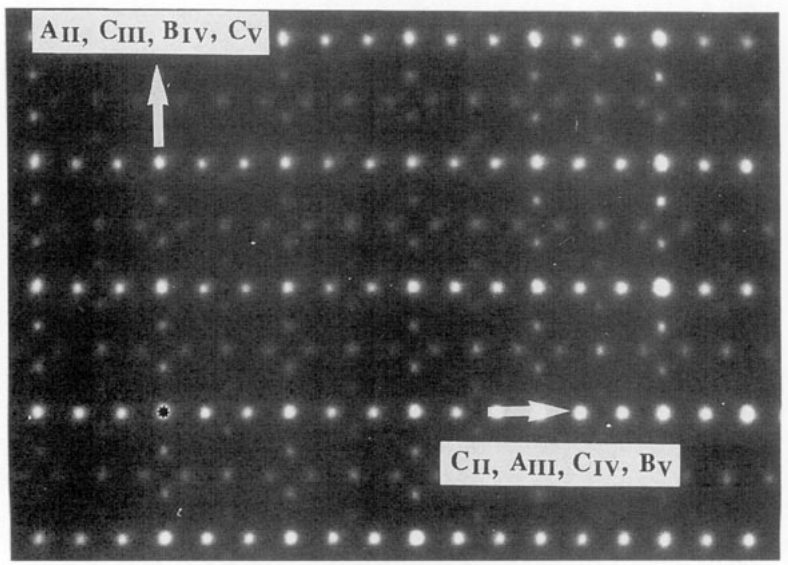

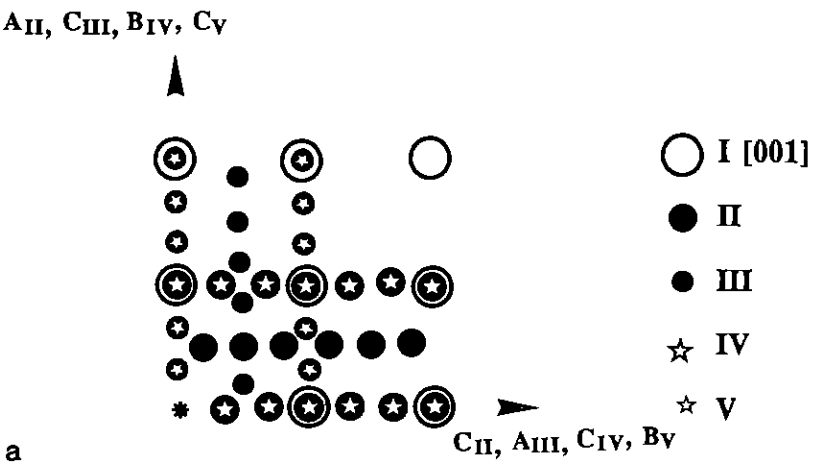

FIG. 9. (a) Complex ED pattern resulting from the superimposition of five components as interpreted on attached drawing. (b) and (c) HREM images of a microcrystal ($x = 0.4$, $n = 2$ batch) showing oriented domains.

Oriented Domains

A second consequence of the influence of the thermal treatments is observed in the formation of oriented domains. The typical electron diffraction patterns which are observed for samples heated for 2 days are shown in Fig. 9a. This complex diagram results from the superimposition of five components which are [001], [100], and [100] 90° oriented, [010], and [010] 90° oriented. This is illustrated in corresponding HREM images of Figs. 9b and 9c. In Fig. 9b, we observe from right to left: [001] zone, [100] zone, and [010] zone, the $\vec{c}$ axis of the two latters being parallel. The formation of fractures at the connection between two domains is a frequent feature. In Fig. 9c, we observe first two [100] zones which are 90° oriented and a [010] zone; on the edge of the crystal a very small [001] zone is observed in the middle part of the image.

The size of these oriented domains is highly variable and ranges from some hundreds to several thousands of angströms.

Though oriented domains would have been expected less frequent after long thermal treatments, they are still observed, showing that the geometrical relationships $a \approx 2b$ and $c/b \sim 6$ are of importance and allow the superstructure to take place along one of the three equivalent directions of the perovskite subcell. Nevertheless, through-focus series images show that the boundary between domains follows steps parallel to (001) and takes place at

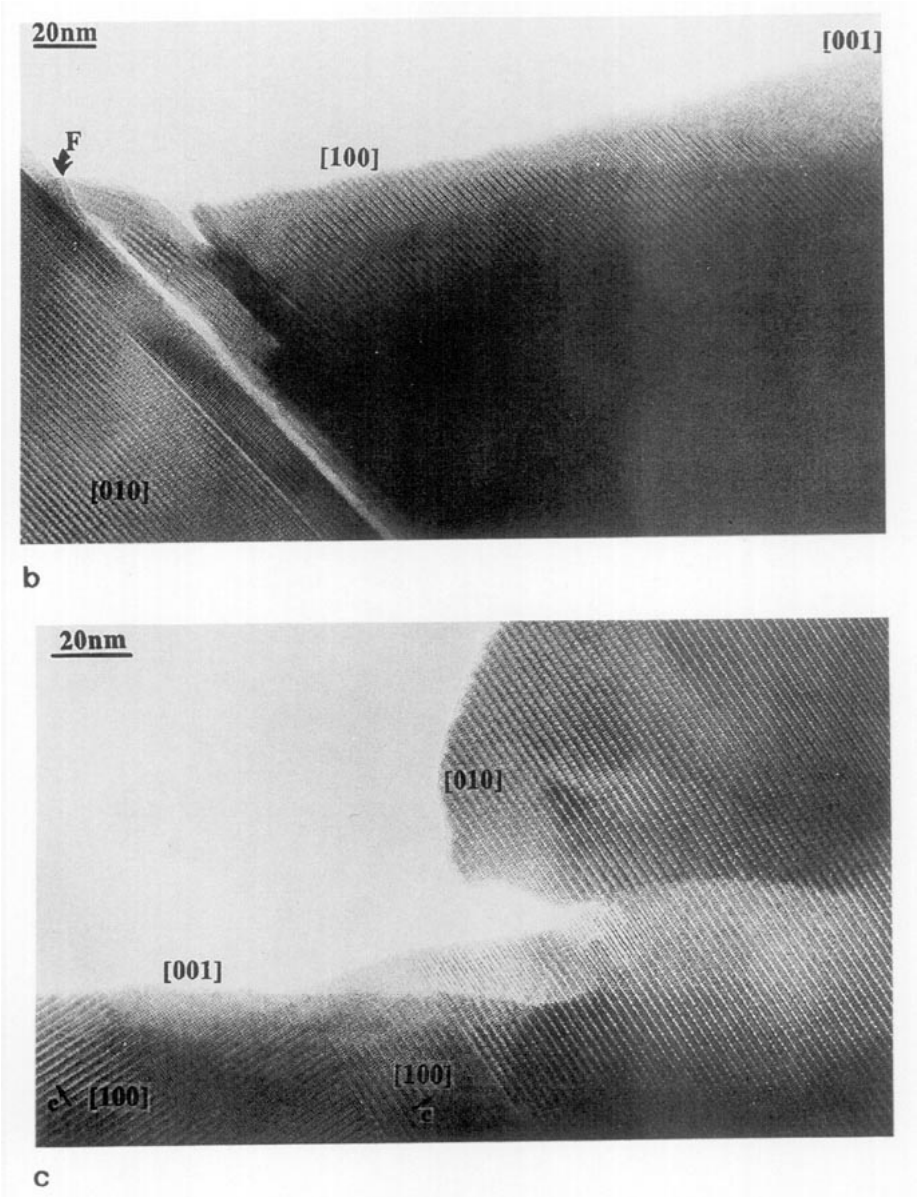

FIG. 9—(*Continued*)

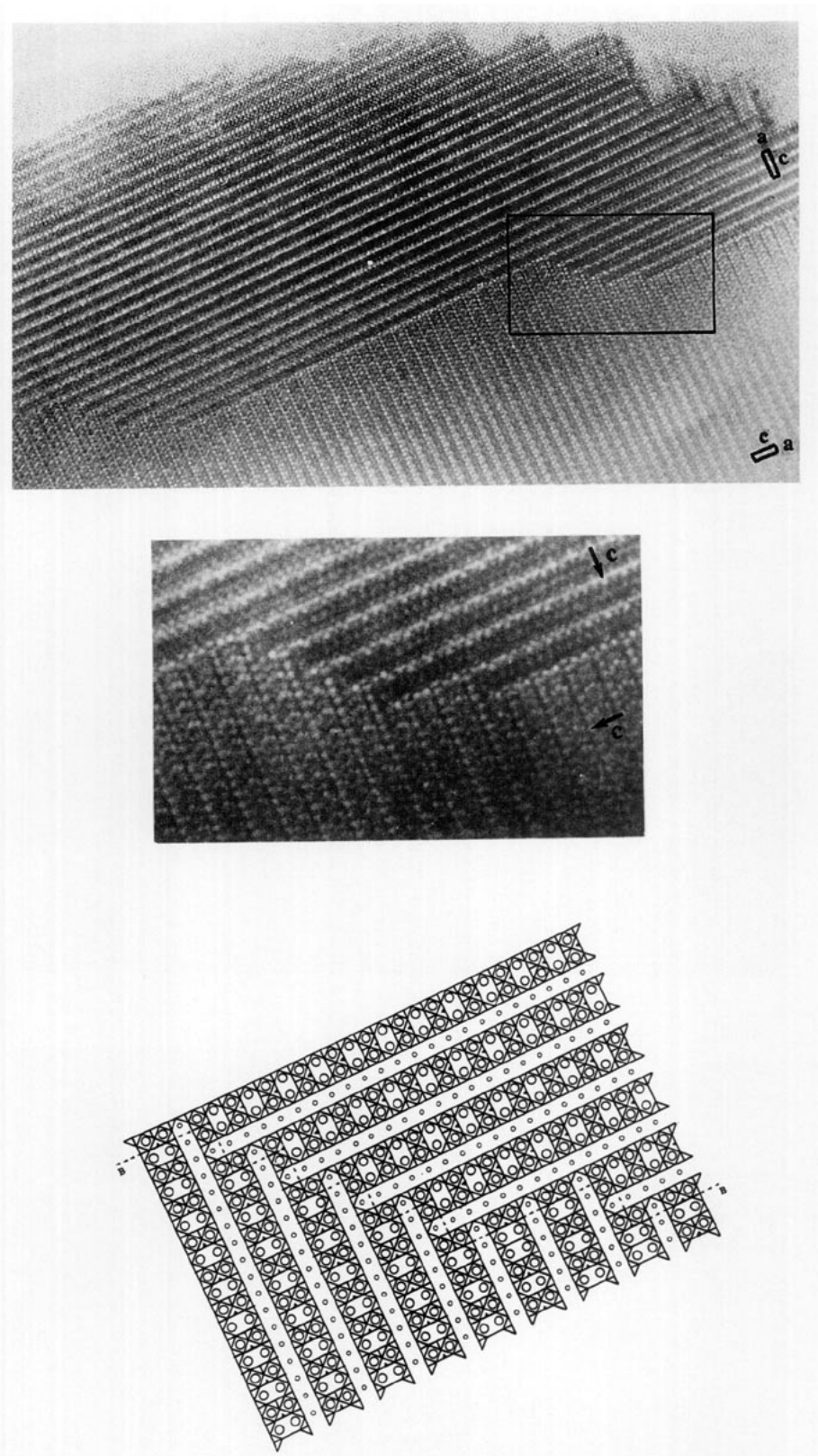

FIG. 10. [010] HREM image of a microcrystal ($x = 0.4$, $n = 2$ batch) exhibiting 90° oriented [010] domains. Detail of the boundary shows steps parallel to (001) which can take place through the carbon-rich layer as in the proposed model.

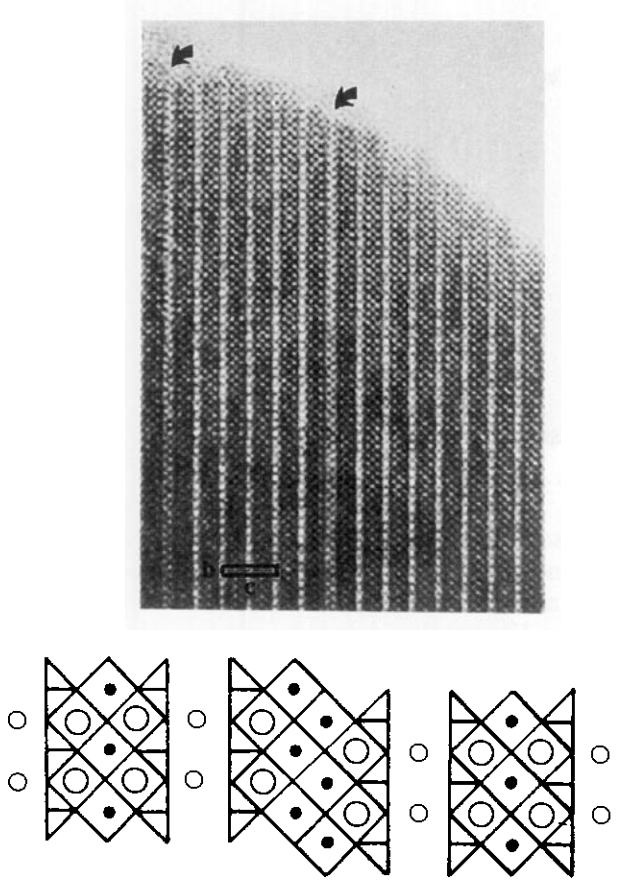

FIG. 11. [100] HREM image of a microcrystal ($x = 0.2$, $n = 6$ batch) showing two layers (arrowed) corresponding to the double row of edge-sharing CuO4 groups of the **124** structure and the corresponding model.

the level of the intermediate mixed carbon–copper layer (Fig. 10). Furthermore, details of a boundary close to the edge of the crystal suggest that the boundary is a carbon-rich layer leading to a model based on an $n = 1$, (Y,Ca) $Ba_2Cu_2CO_7$, layer.

"124"-Intergrowth Defects

Besides the intergrowth of the different n-members, intergrowth with the **124** $YBa_2Cu_4O_8$ structure are sometimes observed. This is illustrated in Fig. 11, for the 0-nm focus value where the copper atoms of $[CuO]_\infty$ layers are imaged as rows of the brightest dots. Indeed, the double row of alternating bright dots in this image (see arrows, Fig. 11) corresponds to the copper atoms of the double row of edge-sharing CuO_4 groups in the **124** structure. This type of intergrowth was very early observed in the pure **123** system Y–Ba–Cu–O (7). Note that such a defect has only been observed here for calcium- and carbon-poor samples.

CONCLUDING REMARKS

This study shows the great influence of calcium substitution in **123** oxycarbonates: in the Ca-free Sr-based compounds the most stable phase seems to be the $n = 4$ member characterized by the "$4a_{123} \times b_{123} \times 2c_{123}$" superstructure (3), whereas in the Ca-doped oxycarbonates, as well as the Ba-based and Sr-based, the stable member corresponds to $n = 2$, with the "$2a_{123} \times b_{123} \times 2c_{123}$" superstructure. The second significant result deals with the large possibility of nonstoichiometry in this system. Indeed, one does not observe a mixture of phases corresponding to n greater than 2, but intergrowths of the **123** structure ($n = \infty$) with the $n = 2$ member, and also at a smaller scale with the $n = 3$ and $n = 1$ members. Moreover, one must emphasize the influence of short thermal treatments on the formation of small modulated zones.

REFERENCES

1. Y. Miyazaki, H. Yamane, N. Ohnishi, T. Katjitani, K. Hiraga, Y. Morii, S. Funahashi, and T. Hirai, *Physica C* **198,** 7 (1992).
2. J. Akimitsu, M. Uehara, M. Ogawa, H. Nakata, K. Tomimoto, Y. Miyazaki, H. Yamane, T. Hirai, K. Kinoshita, and Y. Matsui, *Physica C* **201,** 320 (1992).
3. B. Domengès, M. Hervieu, and B. Raveau, *Physica C,* **207,** 65 (1993).
4. B. Raveau, M. Huvé, A. Maignan, M. Hervieu, C. Michel, B. Domengès, and C. Martin, *Physica C,* **209,** 163 (1993).
5. M. Hervieu, Ph. Boullay, B. Domengès, A. Maignan, and B. Raveau, *J. Solid State Chem.* **105,** 300 (1993).
6. P. A. Stadelmann, *Ultramicroscopy* **14,** 149 (1981).
7. B. Domengès, M. Hervieu, C. Michel, and B. Raveau, *Europhys. Lett.* **4,** 211 (1987).